CrystEngComm

ROYAL SOCIETY OF CHEMISTRY

www.rsc.org/crystengcomm

CrystEngComm RSCPublishing

ARTICLE

Cite this: DOI: 10.1039/x0xx00000x

Received 00th January 2014,
Accepted 00th January 2014

DOI: 10.1039/x0xx00000x

www.rsc.org/

Pyroelectric and Second Harmonic Response from $LiTaO_3$ Nanocrystallites Evolved in Li_2O–B_2O_3–Ta_2O_5 Glass System

P. W. Jaschin and K. B. R. Varma*

Dendritic growth of trigonal and square bipyramidal structures of $LiTaO_3$ nanocrystallites, of 19–30 nm size, was observed when $1.5Li_2O$–$2B_2O_3$–$0.5Ta_2O_5$ glasses were subjected to controlled heat treatment between 530°C–560°C/3h. X-ray diffraction and Raman spectral studies carried out on the heat-treated samples confirmed the formation of $LiTaO_3$ phase along with a minor phase of ferroelectric $Li_2B_4O_7$. The sample that was heat-treated at 550°C/3h was found to possess ~26 nm-sized crystallites which exhibited pyroelectric coefficient as high as 15 nC/cm^{2}K which is in the same range (23 nC/cm^{2}K) as that of single crystalline $LiTaO_3$ at room temperature. The corresponding figures of merit that were calculated for fast pulse detector (F_i), large area pyroelectric detector (F_v) and pyroelectric point detector (F_D) were 0.517×10^{-10} m/V, 0.244 m^2/C and 1.437×10^{-5} Pa$^{1/2}$ respectively. Glass nanocrystal composites comprising ~30 nm-sized crystallites exhibited broad Maker fringes and the second harmonic intensity emanated from these was 0.5 times that of KDP single crystals.

Introduction

A plethora of ferroelectric oxides, including $LiNbO_3$,[1] $BaTiO_3$,[2] $Sr_{0.5}Ba_{0.5}Nb_2O_6$,[3] $Ba_2NaNb_5O_{15}$,[4] $SrBi_2Ta_2O_9$,[5] $Bi_2VO_{5.5}$,[6] and $Ba_5Li_2Ti_2Nb_8O_{30}$[7] have been successfully transformed into glasses and glass-ceramics. The glass-ceramic route offers considerable flexibility in generating pore-free ceramics associated with controlled microstructures that facilitate tunability in physical properties. The relatively less expensive technology involved in obtaining multifunctional materials bolsters the possibilities of employing glass-ceramics for a variety of large-scale applications. The multi-functionality displayed by glass-ceramic ferroelectric materials widens the scope of using them for several applications, such as high energy density capacitors,[8] optical frequency doublers,[9] and pyroelectric,[10] piezoelectric,[11] and electro-optic devices,[12] etc. Borate based glass systems are preferred for reasons such as low cost, large hyperpolarizability and deep UV absorption edge besides their high laser damage threshold.

Lithium tantalate ($LiTaO_3$) is ferroelectric at room temperature and possesses interesting physical properties that could be exploited in various applications ranging from electro-optic modulators, surface acoustic wave oscillators, pyroelectric detectors, non-linear optic devices, generation of terahertz radiation etc. $LiTaO_3$ belongs to the rhombohedral space group *R3c* with lattice parameters a = 5.154 Å and c = 13.781 Å at room temperature. It has a remanent polarisation of 50 μC/cm^2 with its ferroelectric-to-paraelectric transition occurring at 610°C.[13,14] The pyroelectric coefficient at room temperature is 23 nC/cm^{2}K.[15] Because of the complexity involved in obtaining defect-free large single crystals, dispersing nanocrystals in polymer[16] or glass matrix seems to be a viable option. However, polymer matrices narrow down the possibilities to low temperature processing. Literature on glasses and glass-ceramics of $LiTaO_3$ is scarce. This may be due to the poor glass-forming ability of $LiTaO_3$ which precludes the use of conventional techniques to obtain pure lithium tantalate glasses. Roller-quenching[1] and sol-gel[17] methods have been successfully employed to obtain pure $LiTaO_3$ glasses at much smaller scale. There were reports in the literature on the crystallization of $LiTaO_3$ in Li_2O–Ta_2O_5–SiO_2–Al_2O_3 bulk glasses.[18,19] It was observed in this system that there was an impurity phase of $LiAlSi_2O_6$ that evolved along with the desired $LiTaO_3$ phase on heat treatment at appropriate temperature. Indeed in this process high temperature (1600°C) was required to melt the precursors. Interestingly, $LiTaO_3$

---

*Author for communication
Materials Research Centre, Indian Institute of Science, Bangalore-560012, India..
E-mail: kbrvarma@mrc.iisc.ernet.in; Fax: +91 80 2360 0683; Tel: +91 080 2293 2914.

crystallization was accomplished in a borate based reactive glass matrix of $LiBO_2$–Ta_2O_5.[20] However the matrix limited the amount of Ta_2O_5 that could be added to obtain $LiTaO_3$ phase as a result of the chemical reaction between these two. Moreover, in this case, a centrosymmetric $LiBO_2$ phase was also observed to crystallize along with $LiTaO_3$ which affected the desired ferroelectric or non-linear optical properties of the system.

In this article, we report the details pertaining to the fabrication of borate based $LiTaO_3$ glasses and glass nanocrystal composites along with various physical properties that include thermal, dielectric, pyroelectric, ferroelectric and non-linear optical. The base glass system was chosen in such a way that it yielded nanocrystallites of $LiTaO_3$ along with a minor phase of non-centrosymmetric, polar $Li_2B_4O_7$ depending on heat treatment temperature, which we believe participated in bringing out an improvement in physical properties.

Experimental

Optically transparent glasses in the $1.5Li_2O$–$2B_2O_3$–$0.5Ta_2O_5$ system (which on isothermal heat treatment yielded $LiTaO_3$ along with $Li_2B_4O_7$) were fabricated via the conventional melt-quenching technique. For this, Li_2CO_3 (S.D. Fine Chemical, 99%), Ta_2O_5 (Aldrich, 99.99%) and H_3BO_3 (Emparta ACS, 99.5%) were chosen in the respective molar ratio and melted in a platinum crucible at 1300°C for around 30 min in an electric furnace (Lenton). The batch weight was 8 g. The melt was then quickly poured on a steel plate (the temperature of which was maintained at 150°C) and pressed by another plate. A transparent plate of around 20 mm in diameter and 1 mm in thickness was obtained. This was annealed at 250°C (well below the glass transition temperature) for about 5 h to minimize the thermal stresses (if any) associated with it. This was cut into rectangular plates and mirror polished prior to optical and electrical studies. Heat treatment was performed for this composition at 530, 540, 550 and 560°C for 3 h at a heating rate of 3°C/min and furnace cooled, to induce nanocrystallization with varying crystallite sizes and volume fraction of crystallization.

Thermal properties of the as-quenched glasses were studied using differential scanning calorimetry (Perkin Elmer Diamond DSC) covering 50–650°C temperature range. Structural studies on the as-quenched and heat-treated samples were performed using PanAlytical X-pert Pro X-ray diffractometer at room temperature using Cu-K_α radiation operating at 40 kV/30 mA. Densities of the as-quenched and heat-treated samples were measured, with an accuracy of ± 0.01 g/cm^3, using Archimedes' principle and xylene was used as a buoyancy medium. Volume fraction of crystallization of $LiTaO_3$ phase of heat-treated samples was determined from XRD data using KCl as standard (1:1 weight ratio) since there was no overlap of diffraction peaks between them. The volume fraction of crystallization of $LiTaO_3$ was determined from XRD by considering the strong intensity diffraction peak using the following formula[21]

$$x = \left(\frac{x_{KCl}}{k_i}\right)\left(\frac{I}{I_{KCl}}\right) \tag{1}$$

where x_{KCl} is the percentage of KCl (reference material), k_i corresponds to the reference intensity ratio of the strongest diffraction lines of the mixture of polycrystalline $LiTaO_3$ powder and KCl, I and I_{KCl} are the intensities of the diffraction peaks of the mixture of the partially crystallized glass-ceramics and KCl, respectively. Microstructural and structural studies were conducted with the help of FEI Inspect F50 scanning electron microscope and JEOL 2100F transmission electron microscope, respectively. Raman spectra were recorded for the as-quenched and heat-treated samples at room temperature in the range of 50–1200 cm^{-1} using a Raman spectrometer (WiTec Alpha 300) in 180° back-scattering geometry. A frequency doubled Nd-YAG (532 nm) laser was used as the excitation source and the spectral resolution associated with was 3 cm^{-1}.

The dielectric measurements were made using impedance gain phase analyzer (Agilent 4194A HP) with a signal strength of 0.5 V_{rms} in the frequency range of 40 Hz to 110 MHz. Electrical contacts were made by sputtering gold on either side of the flat plate of the as-quenched and heat-treated samples and silver epoxy was used to attach silver leads. Pyroelectric measurements were made on the heat-treated samples using Byer and Roundy method[22] at a heating rate of 3°C/min and pyroelectric current was recorded using Keithley 6485 picoammeter. Polarization-electric field hysteresis measurements were carried out using ferroelectric test system at 500 Hz (Precision Premier II, Radiant Technologies Inc, Albuquerque, NM).

Optical transmission spectra were recorded for the polished as-quenched glass using double-beam UV-Vis spectrophotometer (Perkin-Elmer Lambda 750 UV/Vis/NIR spectrophotometer) in the range of 200–2500 nm. Second harmonic generation (SHG) signals for different heat-treated samples were recorded using the fundamental wave of pulsed Nd-YAG laser operated at 1064 nm, producing 10 ns pulses at 10 Hz, and recorded in transmission mode using a monochromator in conjunction with a photomultiplier tube at room temperature. The incident beam was parallel and its power was close to 1.13 W. The SHG intensities recorded for the heat-treated samples were normalized with respect to the first intense peak obtained on rotating (*00l*) face of a KDP single-crystal of thickness 0.65 mm. All the samples used were of the same thickness. Refractive index of the glass was determined using Brewster angle technique at $\lambda = 532$ nm.

Results and Discussion

Differential scanning calorimetry (DSC) thermogram (Fig. 1(a)) was recorded to assess the desired phase formation temperature in the as-quenched glasses. The DSC curve exhibit one endotherm followed by two distinct exotherms that are ascribed to the glass transition (T_g) and crystallization temperatures (T_{cr1} and T_{cr2}), respectively. The glass transition

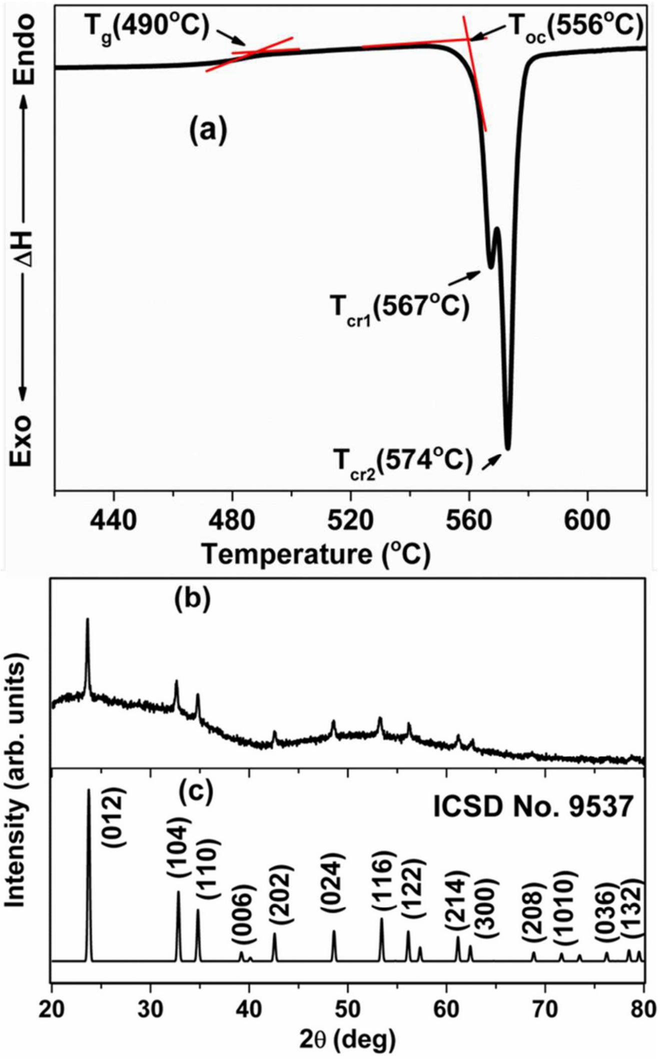

Fig. 1 (a) DSC curve for the as-quenched glass, (b) XRD pattern for the as-quenched sample of $1.5Li_2O–2B_2O_3–0.5Ta_2O_5$ after a DSC run till 570°C at a rate of 10°C/min and (c) the standard XRD pattern for $LiTaO_3$ from ICSD (for quick reference).

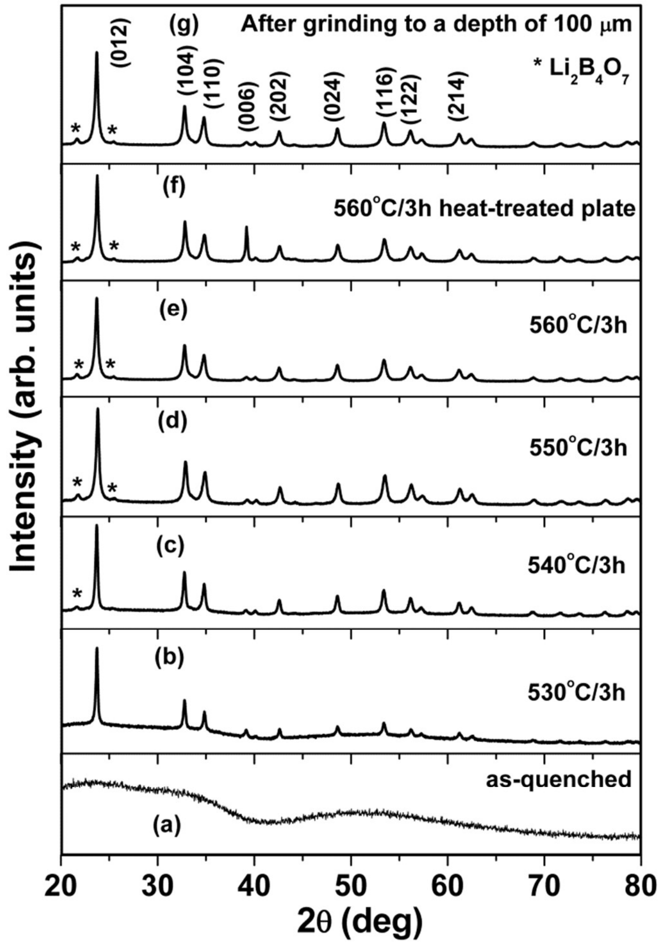

Fig. 2 XRD patterns recorded for the (a) as-quenched glass, (b)–(e) powdered heat-treated glasses at different temperatures and (f) and (g) represent the XRD patterns of 560°C/3h heat-treated glass plate before and after grinding, respectively.

temperature is around 490°C and the crystallization temperatures are 567°C and 574°C. The two exothermic peaks (T_{cr1} and T_{cr2}) encountered for the as-quenched glass are sharp and hence indicate the crystallization of two phases (attributed to the crystallization of $LiTaO_3$ and $Li_2B_4O_7$, based on XRD studies the details of which are illustrated in the subsequent section). The onset of crystallization is 556°C and the thermal stability against crystallization is 77°C for the present composition. The thermal stability is a gross measure of the ability of the glass to delay nucleation and growth process in the system. It is the difference in the crystallization (T_{cr}) and the glass transition temperature (T_g). It is to be noted that the thermal stability of the present glasses is relatively low indicating that there is a high probability of crystallization of a phase just above the glass transition temperature. As the glass transition is heating rate dependent and the exothermic peaks (T_{cr1} and T_{cr2}) are very close to each other, it is suspected that heating the glass around the onset of crystallization (T_{oc}) would yield the desired phase. To begin with, a fast DSC scan (at 10°C/min) was made up to 570°C and cooled down to room temperature. X-Ray powder diffraction pattern obtained for the aforementioned sample (after the DSC run) exhibited diffraction peaks closely matching with that of $LiTaO_3$ phase and no peaks pertaining to any other crystalline phases were observed. The ICSD standard pattern for $LiTaO_3$ is also depicted in Fig. 1(c) for quick reference. However, the hump that is associated with this pattern confirms the existence of amorphous phase. This result strongly suggests that one could overcome the formation of $Li_2B_4O_7$ crystalline phase if the glass is subjected to fast heating rate. The crystallite size associated with this sample was found to be ~15–17 nm and the glass nanocrystal composites obtained at this stage of heating did not exhibit very promising non-linear optical property (second harmonic generation). In order to have further insight into the heat-treatment temperature dependent crystalline phases the as-quenched glasses were heat-treated at 530, 540, 550 and 560°C for 3 h (at 3°/min) which are above the glass transition temperature.

The X-ray powder diffraction patterns obtained for the as-quenched and heat-treated glasses are shown in Fig. 2(a–g).

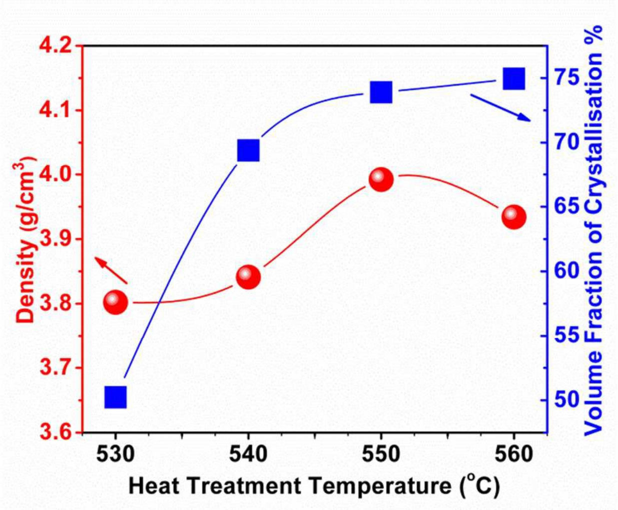

Fig. 3 Plot of variation of density and volume fraction of crystallization of $LiTaO_3$ with heat treatment temperature.

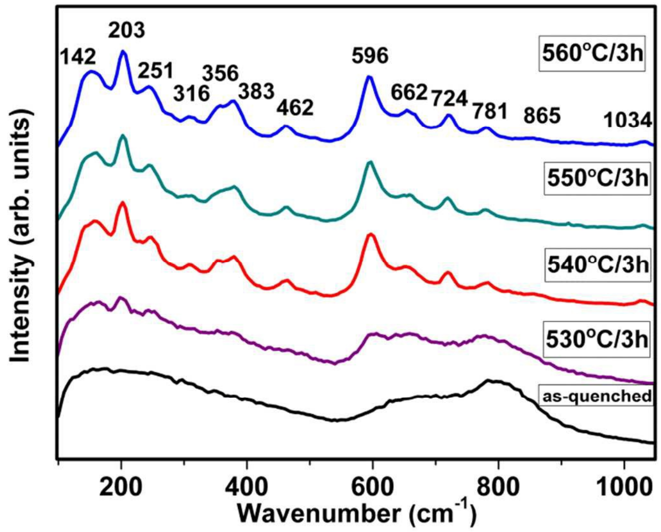

Fig. 4 Raman spectra recorded for the as-quenched and heat-treated glasses of $1.5Li_2O–2B_2O_3–0.5Ta_2O_5$ at various temperatures.

The diffraction pattern for the as-quenched glasses (Fig. 2(a)) is featureless characterizing the presence of short range-order and their amorphous nature. The pattern that is obtained for 530°C/3h heated sample is in close agreement with that of polycrystalline $LiTaO_3$ phase.[23] The lattice *d*-spacings are consistent with those of ferroelectric rhombohedral phase (*R3c*) of $LiTaO_3$ associated with the lattice parameters a = 5.139 Å and c = 13.756 Å. The heat treatment at 540°C/3h (Fig. 2(b–e)) and above resulted in an increase in the $LiTaO_3$ diffraction peak intensities along with the formation of a secondary phase (indicated by * in Fig. 2) which is identified with that of $Li_2B_4O_7$. This is also a non-centrosymmetric, ferroelectric and an active non-linear optic material with a space group of $I4_1cd$ and lattice parameters of a = 9.469Å and c = 10.289Å. The XRD pattern of 560°C/3h heat-treated glass plate, as shown in Fig. 2(f), depicts an increased (006) peak intensity compared to the pattern obtained for the powdered glass-ceramics suggesting an oriented grain growth during heat treatment. But the orientation in the system disappeared when the heat-treated glass plate was polished to a depth of 100 µm, suggesting that the grain orientation is confined to the surface of the glass-ceramics.

The quantification of degree of grain orientation was done using Lotgering's factor[24] which is governed by the equation

$$f = (p-p_o)/(1-p_0) \qquad (2)$$

where $p = \Sigma I_{00l}/\Sigma I_{hkl}$ for the grain oriented sample and $p_o = \Sigma I_{00l}/\Sigma I_{hkl}$ for non-oriented polycrystalline powder. The orientation factor is higher for 560°C/3h heat-treated sample (close to 10%) than for the samples heat-treated at lower temperatures which was close to 3–8% (not shown here). The crystallite sizes determined from the XRD pattern (Scherrer formula) taking into account the peaks corresponding to (202), (024) and (116) show a very little increase with the increase in heat-treatment temperature. The samples heat-treated at 530°C/3h and 540°C/3h yielded crystallites of the size ~19 nm and ~22 nm, respectively, whereas the samples heat-treated at 550°C/3h and 560°C/3h had crystallites of the size ~26 nm and ~30 nm, respectively.

The density of the as-quenched glass was determined to be 3.75 g/cm^3 ($\pm$0.01 g/cm^3). The variation of density and volume fraction of crystallization of $LiTaO_3$ with heat treatment temperature is depicted in Fig. 3. The density of the heat-treated samples is found to increase till 550°C and decrease for 560°C heat-treated sample which may be due to the formation of internal cracks and voids resulting from the thermal mismatch between the phases that crystallize. The volume fraction of crystallization of $LiTaO_3$ (as extracted from the X-ray data) increased with heat treatment temperature as depicted in Fig. 3 and almost saturates at a maximum of 75% for 560°C heat-treated sample. It is to be noted that the change in crystallite size with isothermal heat treatment temperature is not as drastic as the change in the volume fraction of crystallization.

In order to corroborate the structural units present in the system, Raman spectra were recorded for the as-quenched and heat-treated samples of the glass system under study (Fig. 4). Thirteen modes ($4A_1$+$9E_1$) are Raman active for pure $LiTaO_3$, out of which ten peaks have been observed for the 560°C heat-treated sample and are indexed accordingly. The as-quenched glass showed three diffused peaks around 203, 650 and 750 cm^{-1}, where the first-one is attributed to TaO_6 octahedral units and the latter ones are representative of BO_3 triangular units.[25–27] As expected, the peaks begin to sharpen and increase in intensity with the increase in crystallization of the phases involved. Nanocrystallinity in the heat-treated systems is depicted by the broadness of the peaks in the spectra. There is no significant variation in the Raman peak shifts with crystallization suggesting a negligible stress effect from the surrounding matrix.[28] The peak at 596 cm^{-1} (A_1 mode) is assigned to Ta–O stretching involving oxygen atom shifts. The peaks at 203 and 316 cm^{-1} are attributed to the deformation in TaO_6 network mainly by oxygen shifts and Li shifts, respectively. Ta–O bending is characterized by the peak around 462 cm^{-1} and the one at 251 cm^{-1} is mainly due to Li–O framework and Li–O

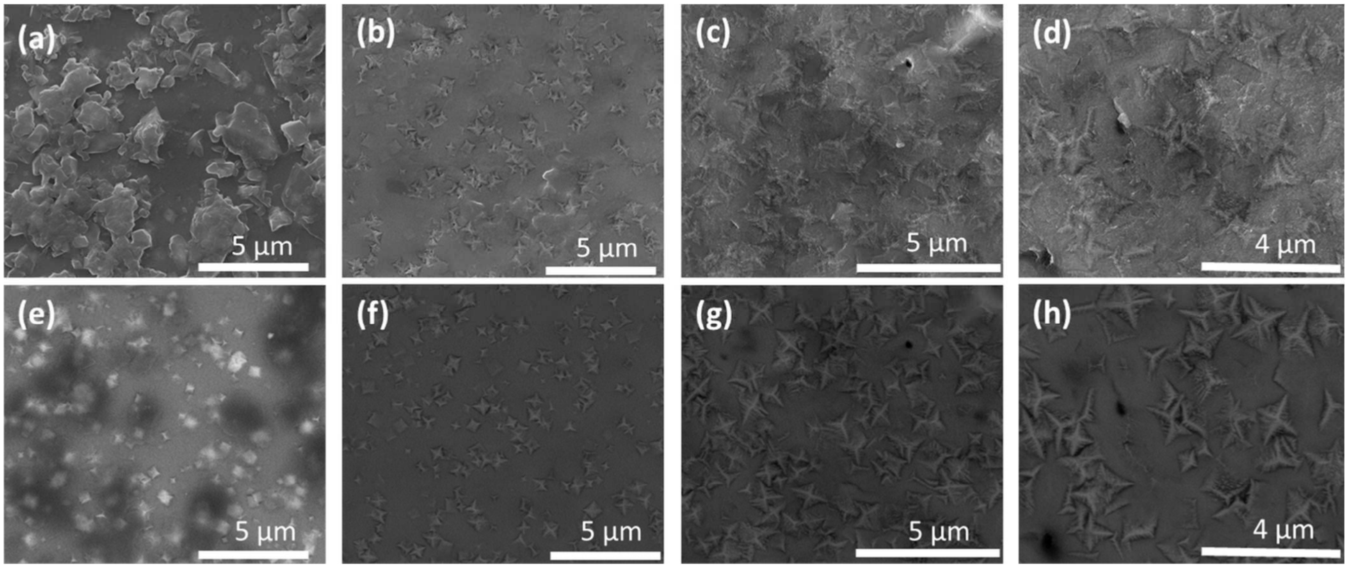

Fig. 5 SEM micrographs of (a),(e)530°C/3h, (b),(f) 540°C/3h, (c),(g) 550°C/3h, (d),(h) 560°C/3h heat-treated glasses in secondary electron mode and back-scattered electron mode, respectively.

stretching and O–Li–O bending modes.[26] The BO_3 asymmetric stretching unit of $Li_2B_4O_7$ is identified with the peaks at 724, 781 and 1034 cm^{-1}.[27]

Phase distribution and crystallite morphology were studied for the samples heat-treated at different temperatures using scanning electron microscopy. In addition to secondary electron images (Fig. 5(a–d)), back-scattered electron images (Fig. 5(e–h)) were recorded for obtaining unclouded phase contrast in the glass matrix. Back-scattered electron images were helpful in unraveling the grain morphology without the requirement of any acid etching. The images reveal the presence of $LiTaO_3$ crystallites having a spherulitic and trigonal/square pyramidal structures embedded in the borate matrix. In Fig. 5, both secondary and back-scattered electron images obtained for the same region are depicted. The 530°C heat-treated sample shows the $LiTaO_3$ spherulites embedded deep in the residual glass matrix, with their diameter between 500 nm and 1 µm. The dark regions in the Fig. 5(e) occurs as a result of the phase difference within the region of interest and hence, suggesting an inhomogeneity in the phase distribution. With higher temperature of heat treatment, there is an increase in the size of spherulites up to 2 µm and a reduced inhomogeneous phase distribution is observed. The residual glassy layer also reduces with heat treatment and the star-shaped grains are observed quite distinctly in the secondary electron images for the 550°C and 560°C heat-treated samples. Each spherulite is a centre of nucleation and the rate of nucleation is higher when the heat treatment is close to the glass transition. This could be the reason for the less number of spherulites for the 560°C heat-treated sample as compared to the rest. But the rate of crystal growth exceeds the nucleation rate during heat treatment close to the crystallization temperature inducing a drastic increase in the grain size at 560°C. Fig. 6 depicts the evolution of the grains as a function of heat treatment temperature as recorded in the back-scattered electron mode. The dendritic growth in the spherulites in the 530°C and 540°C are less prominent compared to the 550°C and 560°C heat-treated samples. An apparent needle shaped growth morphology radially distributed from the center of the spherulites is observed for the 530°C heat-treated samples. Whereas 540°C heat-treated samples revealed a combination of needle-shaped and droplets of the crystallites around the spherulite. For this sample, needle-shaped growth appears to break down to droplets of crystallites with varying sizes from 20–50 nm. With 550°C heat treatment, the droplets and needle-shaped growth habits are absent and a more prominent dendritic growth of the crystallites with branching from the edges of the pyramidal structures was observed. More protrusive bipyramidal structures are observed for these systems, rather than the spread-out spherulites. Such dendritic growth of crystallites, resulting from the coalescence of phase-separated regions in a glass matrix has been observed in various other glass-ceramics as reported in the literature, *e.g.*, $LiNbO_3$,[29] $CaMgSi_2O_6$,[30] and YAG-based glass-ceramics.[31,32] Dendritic growth of crystallites suggests that there is a sudden removal of heat from the surface of the glasses. Dendritic growth and concomitant partial grain orientation along [*00l*], as revealed by the X-ray diffraction studies, is attributed to the rapid dissipation of heat along this direction as this is known to be preferred one in these systems.[33]

Fig. 7(a) is a TEM image of the as-quenched glass under study which appears to be featureless as corroborated by the diffused selected area electron diffraction (SAED) pattern shown in Fig. 7(b). The HRTEM image recorded on a more electron transparent region of the as-quenched glass (Fig. 7(c)) reveals the presence of nanocrystallites (with a diameter close to 7 nm) with the lattice spacing (d_{012} = 3.52 Å) matching with that of *(012)* plane of $LiTaO_3$. In Fig. 7(d), nanocrystallites of 25–30 nm in diameter embedded in an amorphous matrix are observed for 560°C/3h heat-treated glass, which is in agreement with that obtained using XRD analysis. As mentioned earlier, the dendritic growth is due to the coalescence of the nanocrystals on heat treatment and the presence of

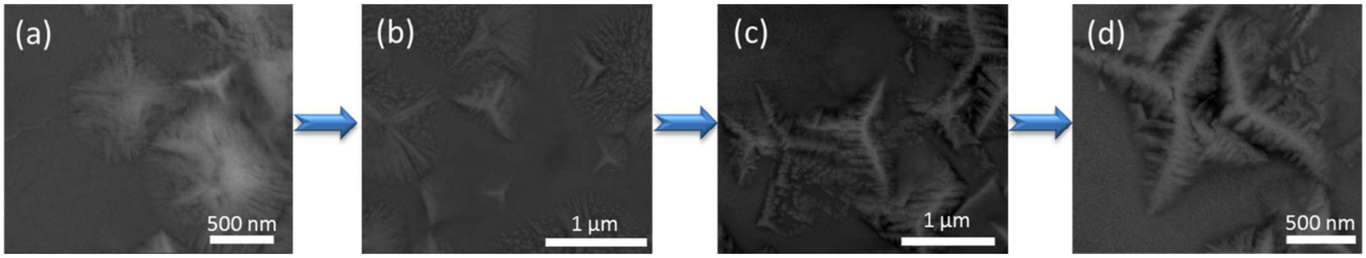

Fig. 6 Back-scattered electron images revealing the sequence of crystal growth at (a) 530°C/3h, (b) 540°C/3h, (c) 550°C/3h, (d) 560°C/3h heat-treatment temperature.

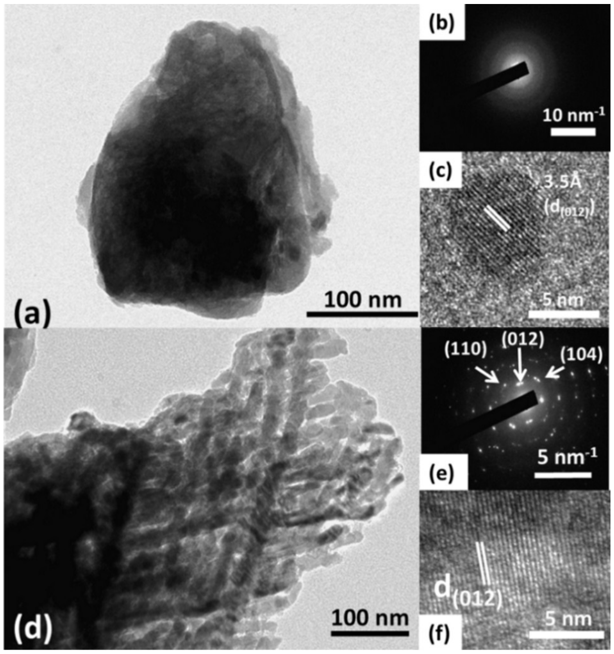

Fig. 7 TEM images of the (a) as-quenched glass and (d) 560°C/3h heat-treated glass; SAED pattern and HRTEM image of (b), (c) as-quenched glass and (e), (f) 560°C/3h heat-treated sample, respectively.

nanocrystallites in Fig. 7(d) confirms this phenomenon of self-assembled nanocrystals. Coalescence occurs when a large crystallite appears to have formed due to the necking of two smaller nanocrystallites.[34] This necking is observed in the image resulting in an elongated appearance of the nano-crystals. The corresponding SAED pattern depicts spotty rings indicating polycrystallinity in the system (Fig. 7(e)) and is indexed to $LiTaO_3$ phase. The lattice fringes obtained from HRTEM (depicted in Fig. 7(f)) are in close agreement with the *d*-spacing of *(012)* plane of $LiTaO_3$ (depicted in Fig. 7(f)).

The tunability of physical properties in glass-ceramics provides a platform for the materials to be used for multiple applications. In this regard, the variation of dielectric constant with respect to crystallization is a factor to be of prime importance. The variation of dielectric constant (ε_r) and loss (D) at room temperature at 100 kHz as a function of heat treatment temperature of the glasses is given in Table I. The dielectric constant and loss for the as-quenched glass at 100 kHz was found to be 20.63 and 0.044, respectively. The dielectric constant increased while the loss decreased with heat treatment temperature and attained a dielectric constant maximum of 25 and minimum loss of 0.017 for 560°C heat-treated sample at 100 kHz. The dielectric constant of a composite is primarily dependent on the phase distribution and volume fractions of the constituents. Hence, with increase in the volume fraction of $LiTaO_3$, that possesses a higher dielectric constant at room temperature (ε_r = 47)[15] relative to the glass matrix, the dielectric constant does increase. The high loss for the as-quenched glass is due to the Li^+ ion migration across the glass network. However, after crystallization the systematic decrease in the loss is due to the confinement of the Li^+ ions across the interfacial region between the glass and the nanocrystals. The variation in dielectric constant with crystallization has not been very significant but the change in loss has been drastic, which could be very advantageous in the perspective of its pyroelectric properties since the pyroelectric figures of merit depend inversely on the dielectric constant and loss.

The pyroelectric coefficient was determined using Byer and Roundy technique in the temperature range 25–150°C at a heating rate of 3°C/min. The pyroelectric current and pyroelectric coefficient are governed by the equation

$$I = Ap(T)\left(\frac{dT}{dt}\right) \qquad (3)$$

where *A* is the electroded area of the sample, *p(T)* is the pyroelectric coefficient and *dT/dt* is the heating rate. Pyroelectric coefficient of the heat-treated samples (530–560°C/3h) as a function of temperature is shown in Fig. 8. The trend in the variation of pyroelectric coefficient with temperature has been consistent for all the heat-treated samples and a higher pyroelectric coefficient is observed for the heat-treated glasses comprising higher volume fraction of $LiTaO_3$ crystallites. The pyroelectric coefficient of 550°C/3h heat-treated sample is as high as 15 nC/cm^2K at 30°C. At 100°C, a pyroelectric coefficient of 90 nC/cm^2K was achieved for 560°C heat-treated sample. Such magnitude of pyroelectric coefficient observed in glass-ceramics is interesting, considering the single crystal pyroelectric coefficient of $LiTaO_3$ is only 23 nC/cm^2K at room temperature. Whereas, there is an additional pyroelectric phase of $Li_2B_4O_7$ for which the pyroelectric coefficient is found to be 3 nC/cm^2K at room temperature.[35] Moreover, pyroelectric coefficients in glass-ceramics are, generally, of secondary effect in nature which is caused by local stress induced polarisation change endured by the thermal expansion mismatch between the crystallites and the residual glass matrix. Such secondary effects could be observed even without poling the samples.[36] However, Halliyal et al.[37] proposed that tailoring pyroelectric and piezoelectric properties of polar glass-ceramics is possible by orienting the crystallites. Properties close to that of single crystalline materials could be achieved by appropriate modification of the crystalline orientation. About 75% of the pyroelectric coefficient of a single crystalline material was achieved for a fresnoite-based oriented glass-ceramics.[37] In this regard, the *(00l)* orientation on the sample surface caused by the inherent temperature gradient during heating might have resulted in orienting the local dipoles in the system since *c*-axis remains the polar axis of $LiTaO_3$. Here, the partially oriented diploes on the sample surface along with better connectivity of the crystallites due to the dendritic structures provide the basis for the large magnitude of pyroelectric coefficient along with the added innate secondary pyroelectric effects in the system.

The figures of merit for an uncooled pyroelectric IR detector for different applications are governed by the equations[38]

Fast pulse detector, $F_i = \frac{p}{c_v}$

Large area detector, $F_v = \frac{p}{c_v \varepsilon_0 \varepsilon_r}$

Pyroelectric point detector, $F_D = \frac{p}{c_v \sqrt{\varepsilon_0 \varepsilon_r tan\delta}}$

where p is the pyroelectric coefficient, c_v is the volume specific heat of the sample determined using DSC and ε_o is permittivity of free space (8.854×10^{-12} F/m). The figures of merit obtained using the above formulae for the heat-treated glasses are listed in Table I. To reinforce the polar nature of the heat-treated samples, they were subjected to P *vs*. E ferroelectric hysteresis loop studies and the recorded loops are shown in Fig. S1. The loops appear lossy due to relatively high ionic conductivity associated with the samples. The remnant polarisation of 550°C/3h heat-treated sample showed a $2P_r$ value of 0.83 μC/cm^2 and a coercive field of 74 kV/cm. All the parameters associated with the ferroelectric studies are also illustrated in Table I.

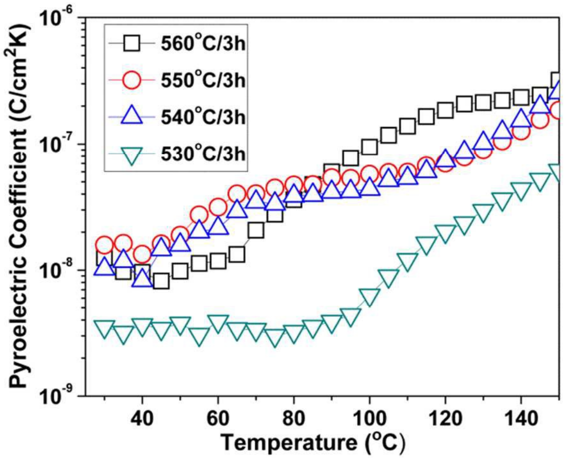

Fig. 8 Pyroelectric coefficient variation as a function of temperature for the heat-treated samples of $1.5Li_2O–2B_2O_3–0.5Ta_2O_5$.

Optical transmission spectra recorded (Fig. S2) in the 200–2500 nm wavelength range for the as-quenched glass shows around 65% transmission in the visible and infrared range. The optical energy band-gap (E_{opt}) was evaluated from Tauc's plot in which

$$\alpha(\nu) = const[(h\nu - E_{opt})^2/h\nu] \qquad (4)$$

where $\alpha(\nu)$ is the absorption coefficient and h is the Planck's constant. From the *x*-intercept of the straight line in the plot of ln($\alpha(\nu)$) vs $h\nu$ (shown as the inset in Fig. S2) the optical energy band-gap was estimated to be 4.32 eV (±0.01 eV). The refractive index at 532 nm (determined using Brewster's angle technique) for the as-quenched glass was found to be 1.77.

The presence of spontaneous polarisation in the glass-ceramic system must also induce a second harmonic generation (SHG) in the system. Fig. 9(a) displays the angular variation of second harmonic generation intensity (532 nm) obtained for the 560°C heat-treated sample at 1064 nm. A broad spectrum with maxima at normal incidence was observed indicating a strong scattering from the system.

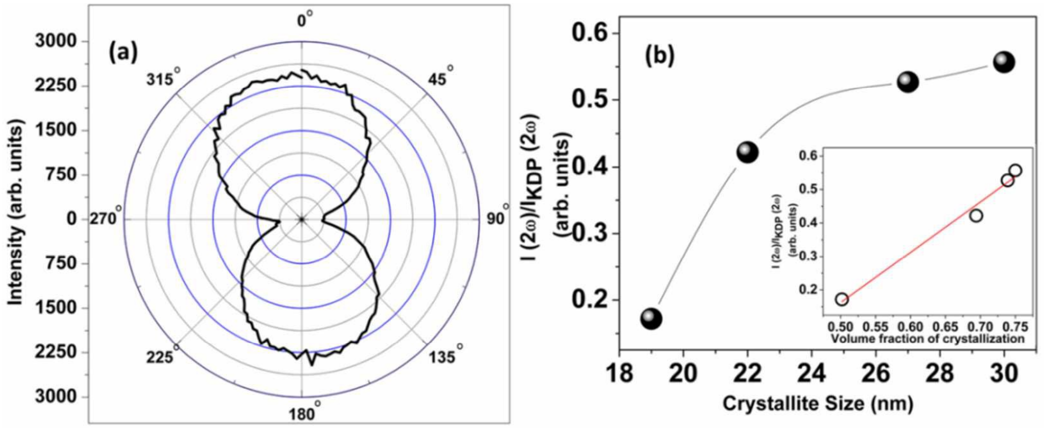

Fig. 9 (a) Polar plot of second harmonic intensity of 560°C/3h heat-treated glass as a function of incident angle. (b) Normalized SHG intensity of the glass as a function of crystallite size and the inset shows the variation of SHG intensity as a function of volume fraction of crystallization of $LiTaO_3$.

Table I. Dielectric constant (ε_r), loss (D), remnant polarisation (P_r), coercive field (E_c), pryoelectric coefficients (*p*) and pryoelectric figures of merit for heat-treated samples of $1.5Li_2O–2B_2O_3–0.5Ta_2O_5$.

Heat treatment temperatures °C	**ε_r at 100 kHz**	**D at 100 kHz**	**$2P_r$ μC/cm^2**	**E_c kV/cm**	**Pyroelectric coefficient nC/cm^{2}K at 30°C**	**F_i Fast pulse detector x 10^{-10} m/V**	**F_v Large area detector m^2/C**	**F_D Point detector x 10^{-5} Pa$^{1/2}$**
530	21.39	0.107	0.61	46	3.53	0.127	0.067	0.282
540	22.23	0.079	0.82	55	10.25	0.357	0.181	0.905
550	23.97	0.061	0.83	74	15.28	0.517	0.244	1.437
560	25.14	0.017	0.59	55	14.53	0.435	0.196	2.236

All the heat-treated samples exhibited SHG response. The samples heat-treated at 540°C and above were highly translucent to visible light, with a transmission of less than 5% which is due to high scattering loss at the interfaces of two crystalline phases associated with different refractive indices. The normalized second harmonic intensity as a function of crystallite size is shown in Fig. 9(b). Intensity half as much as that obtained for KDP single crystal of the same thickness was observed for 30 nm-sized crystallites of 560°C heat-treated sample. This indicates a strong enhancement in the SHG intensity with the increase in volume fraction of crystallized $LiTaO_3$ as shown in the inset of Fig. 9(b). A linear relationship between the volume fraction of $LiTaO_3$ crystallites and the second harmonic intensity is observed as shown in the inset of Fig. 9(b) and is suggestive of the occurrence of hyper Rayleigh scattering in the medium.[39] If so, it is possible that the SHG response is an additive effect of intensities arising out of individual spherulites in the glass nanocrystal composites.[29] A more detailed study in this regard is in progress. Moreover, the presence of $Li_2B_4O_7$ nano-crystallites could also enhance the frequency conversion as the d_{33} of its single crystalline counterpart is about 3 times that of d_{11} of quartz.[40] The growth of large spherulites in the glass system on heat treatment mars the possibility of better transparency in the system. But being a strong scattering system, it has not completely deteriorated its frequency conversion efficiency. However, it has been observed in polycrystalline[41,42] and strongly scattering media[43,44] that the SHG efficiency is rather enhanced by a random phase matching process where the output second harmonic intensity of the generated wave is resulted from the sum of the intensities arising from individual domains or grains. An enhanced SHG signal could, thus, be as a result of the interference of scattered light.[43]

Conclusions

Nanocrystallization of industrially important pyroelectric $LiTaO_3$ was accomplished in $1.5Li_2O–2B_2O_3–0.5Ta_2O_5$ glass by subjecting it to isothermal heat-treatment in the 530–560°C temperature range for 3h. XRD and Raman spectroscopy confirmed the crystallization of desired $LiTaO_3$ along with $Li_2B_4O_7$ as an impurity phase. Dendritic growth of $LiTaO_3$ nanocrystallites, as a consequence of coalescence of nanocrystals, is revealed by SEM and TEM studies. A pyroelectric coefficient as high as 15 nC/cm^{2}K was exhibited by the sample comprising 26 nm-sized crystallites obtained after 550°C/3h heat treatment. These samples exhibited P-E hysteresis loops associated with $2P_r$ and E_c of 0.83 μC/cm^2 and 74 kV/cm, respectively. Second harmonic generation was observed for all the samples under investigation for a fundamental wavelength of 1064 nm. The SHG intensity was 0.55 times that of KDP single crystal.

Acknowledgements

The authors acknowledge Prof. K.K. Nanda and Subrata Senapati for their help in recording Raman spectra.

References

1. A. M. Glass, M. E. Lines, K. Nassau and J. W. Shiever, *Appl. Phys. Lett.,* 1977, **31,** 249.
2. K. Tanaka, H. Kuroda, A. Narazaki, K. Hirao and N. Soga, *J. Mater. Sci. Lett.,* 1998, **17,** 1063.
3. T. Yamazawa, T. Honma, H. Suematsu and T. Komatsu, *J. Am. Ceram. Soc.,* 2009, **92,** 2924.
4. S. Kundu and K.B.R. Varma, *Cryst. Growth Des.,* 2014, **14,** 585.
5. G. S. Murugan and K. B. R. Varma, *J. Mater. Chem.,* 2002, **12,** 1426.
6. M. V. Shankar and K. B. R. Varma, *J. Non-Cryst. Solids,* 1994, **167,** 247.
7. M. N. Ahamad and K. B. R. Varma, *Dalton Trans.,* 2010, **39,** 4624.
8. E.P. Gorzkowski, M.J. Pan, B. Bender and C.C.M. Wu, *J Electroceram.,* 2007, **18**, 269–276
9. H. Tanaka, M. Yamamoto, Y. Takahashi, Y. Benino, T. Fujiwara, and T. Komatsu, *Opt. Mater.,* 2003, **22**, 71–9
10. M. M. Layton and J. W. Smith, *J. Am. Ceram. Soc*., 1975, **58**, 435.
11. M. Patschger, W. Wisniewski and C. Russel, *CrystEngComm*, 2012, **14**, 7368.

12. N.F. Borrelli, A. Herczog, and R. D. Maurer, *Appl. Phys. Lett.*, 1965, **7**, 117.
13. S.H. Wemple, M. DiDomenico, and I. Camlibel, *Appl. Phys. Lett.*, 1968, **12**, 6.
14. R. C. Miller and A. Savage, *Appl. Phy. Lett.,* 1966, **9**, 169.
15. R. Vaish, *Int. J. Appl. Ceram. Technol.,* 2012, **9**, 1.
16. P. Guggilla, A. K. Batra, M. E. Edwards, *J Mater Sci,* 2009, **44**, 5469
17. C.G. Baek, H.W. Choi and Y.S. Yang, *J. Alloys Comp*., 2014, **615**, 745.
18. A. Tarafder, K. Annapurna, R. S. Chaliha and B. Karmakar, *Int. J. Appl. Ceram. Technol.,* 2011, **8**, 1031.
19. S. Ito, T. Kokubo, M. Tashiro, *J. Mat. Sci.*, 1978, **13,** 930.
20. P. Mukherjee and K. B. R. Varma, *Ferroelectrics,* 2004, **306,** 129.
21. F.H. Chung, *J. Appl. Crystallogr*., 1974, **7,** 519.
22. R. L. Byer and B. Roundy*, Ferroelectrics*, 1972, **3**, 333.
23. S.C. Abrahams, J.L. Bernstein, *J. Phys. Chem. Solids*, 1967, **28**, 1685.
24. F. K. Lotgering, *J. Inorg. Nucl. Chem.,* 1959, **9,** 113.
25. A. F. Penna, A. Chaves, P. R. Andrade and S. P. S. Porto, *Phys. Rev. B,* 1976, **13**, 11.
26. Y. Repelin, E. Husson, F. Bennani and C. Proust, *J. Phys. Chem. Solids,* 1999, **60,** 819.
27. G. L. Paul and W. Taylor, *J. Phys. C,* 1982, **15,** 1753.
28. W F Zhang, Y.L. He, M.S. Zhang, Z. Yin and Q. Chen, *J. Phys. D: Appl. Phys*., 2000, **33,** 912.
29. H. Vigouroux, E. Fargin, S. Gomez, B.L. Garrec, G. Mountrichas, E. Kamitsos, F. Adamietz, M. Dussauze and Vincent Rodriguez, *Adv. Funct. Mater.* 2012, **22**, 3985.
30. W. Wisniewski, K. Otto, and C. Russel, *Cryst. Growth Des.*, 2012, **12**, 5035.

.

31. A. Keshavarzi, W. Wisniewski and C. Russel, *CrystEngComm,* 2012, **14**, 6904.
32. A. Keshavarzi, W. Wisniewski, R. Kloe and C. Russel, *CrystEngComm,* 2013, **15**, 5425.
33. H. C. Zeng, K. Tanaka, K. Hirao and N. Soga, *J. Non-Cryst. Solids,* 1997, **209,** 112.
34. D. Gruner and Z. Shen, *CrystEngComm*, 2011, **13**, 5303.
35. A. S. Bhalla, L. E. Cross and R. W. Whatmore, *Jpn. J. Appl. Phys.,* 1985, **24,** 727
36. M. Es-Souni, M. Kuhnke, S. Iakovlev, C.H. Solterbeck, and A. Piorra, *Appl. Phys. Lett.,* 2005, **86**, 022907.
37. A. Halliyal, A. S. Bhalla and R. E. Newnham, *Mat. Res. Bull*., 1983, **18**, 1007.
38. J. Zhang, X. Dong, F. Cao, S. Guo and G. Wang, *Appl. Phy. Lett.,* 2013, **102,** 102908.
39. E. Valdez, C.B. de Araujo and A.A. Lipovskii, *Appl Phys Lett.*, 2006, **89**, 031901.
40. S. Furusawa, O. Chikagawa, S. Tange, T. Ishidate, H. Orihara, Y. Ishibashi, and K. Miwa, *J. Phys. Soc. Jpn*., 1991, **60**, 2691.
41. S. E. Skipetrov, *Nature,* 2004, **432**, 285.
42. M. Baudrier-Raybaut, R. Haïdar, Ph. Kupecek, Ph. Lemasson, and E. Rosencher, *Nature,* 2004, **432**, 374.
43. V.A. Mel'nikov, L.A. Golovan, S.O. Konorov, D.A. Muzychenko, A.B. Fedotov, A.M. Zheltikov, V.Y. Timoshenko, P.K. Kashkarov, *Appl. Phys. B*, 2004, **79**, 225.
44. V. E. Kravtsov, V. M. Agranovich, and K. I. Grigorishin, *Phys. Rev. B,* 1991, **44**, 4931**.**

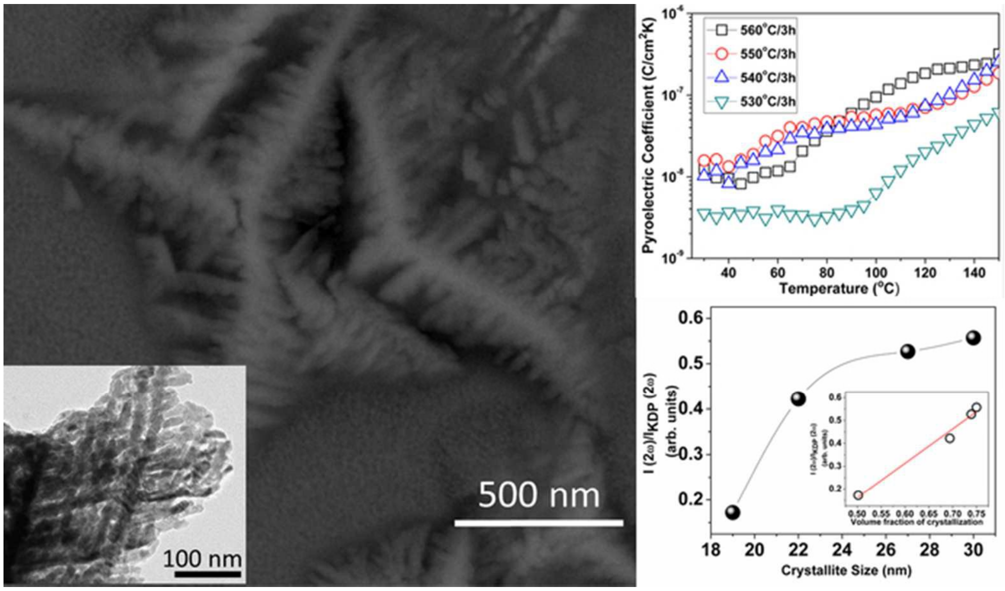

Pyroelectric coefficient and second harmonic generation of nanocrystalline $LiTaO_3$ grown in the form of dendritic spherulites in the glass matrix.
58x34mm (300 x 300 DPI)